

# Two-Digit Robotic Exoskeleton Glove Mechanism: Design and Integration

## Eric Refour

Mem. ASME  
Robotics and Mechatronics Laboratory,  
Electrical & Computer Engineering Department,  
Virginia Tech,  
Blacksburg, VA 24060  
e-mail: erefour@vt.edu

## Bijo Sebastian

Mem. ASME  
Robotics and Mechatronics Laboratory,  
Mechanical Engineering Department,  
Virginia Tech,  
Blacksburg, VA 24060  
e-mail: bijo7@vt.edu

## Pinhas Ben-Tzvi<sup>1</sup>

Mem. ASME  
Robotics and Mechatronics Laboratory,  
Mechanical Engineering Department,  
Virginia Tech,  
Blacksburg, VA 24060;  
Robotics and Mechatronics Laboratory,  
Electrical & Computer Engineering Department,  
Virginia Tech,  
Blacksburg, VA 24060  
e-mail: bentzvi@vt.edu

*This paper presents the design and integration of a two-digit robotic exoskeleton glove mechanism. The proposed glove is designed to assist the user with grasping motions, such as the pincer grasp, while maintaining a natural coupling relationship among the finger and thumb joints, resembling that of a normal human hand. The design employs single degree-of-freedom (DOF) linkage mechanisms to achieve active flexion and extension of the index finger and thumb. This greatly reduces the overall weight and size of the system making it ideal for prolonged usage. The paper describes the design, mathematical modeling of the proposed system, detailed electromechanical design, and software architecture of the integrated prototype. The prototype is capable of recording information about the index finger and thumb movements, interaction forces exerted by the finger/thumb on the exoskeleton, and can provide feedback through vibration. In addition, the glove can serve as a standalone device for rehabilitation purposes, such as assisting in achieving tip or pulp pinch. The paper concludes with an experimental validation of the proposed design by comparing the motion produced using the exoskeleton glove on a wooden mannequin with that of a natural human hand. [DOI: 10.1115/1.4038775]*

## 1 Introduction

Over the past few decades, exoskeletons and haptic gloves have emerged in popularity within the fields of virtual reality (VR) and medical applications. In the realms of VR, exoskeletons and haptic gloves are used to create realistic experiences by generating

tactile responses to reflect the sensation of the user touching an object [1–3]. Within the medical field, exoskeleton gloves are used in numerous ways, such as being an assistive tool for tele-operated surgeries or serving as a rehabilitation tool for people who suffer from paralysis in the hand and/or fingers [4–6]. Unfortunately, many of these commercial gloves are expensive and require complex equipment, making them unwieldy and less portable for activities of daily living (ADLs).

There have been two main approaches for designing exoskeleton gloves throughout the years. Many researchers use the traditional approach toward building an exoskeleton glove, which involves using rigid links and joints to apply forces to the corresponding joints of the human hand to provide assistance with flexion and extension [7–19]. Most of these exoskeleton gloves are designed with the link frames placed on top of the fingers and hand instead of alongside the fingers. This is primarily due to the fact that the size of the link frames exceeds the available space between the fingers. The major drawback of this concept is that it results in a bulky and heavy glove, which can result in increased user fatigue during prolonged operation.

The second commonly used approach toward designing exoskeleton gloves is to replace the rigid mechanisms with softer materials. This approach focuses on using a tendon-driven design [20–23] or elastic polymers as inflatable membranes, which expand to achieve the desired bending profiles similar to that of human fingers [24–26]. Unfortunately, both designs have their share of disadvantages. The soft gloves driven by tendon cables have the following drawbacks: discomfort produced by the pre-tensioning of the cables, loss in efficiency caused by friction along the tendon path, and the creation of shear forces applied onto the soft material by the tendons during flexion and extension. These factors together hinder effective force transmission in tendon-driven systems thereby decreasing their repeatability. On the other hand, the soft inflatable gloves are challenged by their inability to provide natural flexions and extensions profiles for the human finger and are therefore limited to only achieving the basic configurations of fully open or closed fist.

The aim of this paper is to present an exoskeleton glove designed to overcome the previously mentioned drawbacks of traditional rigid and soft exoskeleton gloves. The exoskeleton glove is intended to be general purpose, possessing the ability to serve as a medical device or virtual reality haptic glove. As a proof of concept for the proposed glove design shown in Fig. 1, a two-digit (index finger and thumb) prototype was developed and its functionality was validated through experimental analysis. For the experimental analysis, one of the potential applications of the full glove is explored; an assistive glove providing support for disabled teens/adults. The rest of the paper is organized as follows: the conceptual design and mathematical modeling are described in Sec. 2 while Sec. 3 covers the detailed electromechanical design of the prototype. Section 4 presents the integration of the two-digit prototype and Sec. 5 discusses the experimental results. Section 6 talks about the possible improvements that can be made to the design to extend its functionalities by incorporating electric actuation module. Finally, Sec. 7 concludes the paper.

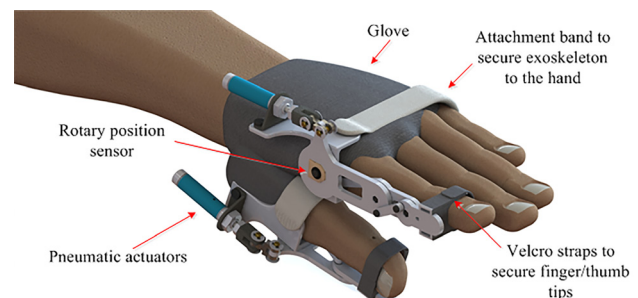


Fig. 1 Proposed design

<sup>1</sup>Corresponding author.

Manuscript received September 21, 2017; final manuscript received December 12, 2017; published online January 29, 2018. Assoc. Editor: Venkat Krovi.



Fig. 2 Anatomy of the human hand

## 2 Mechanical Design

In order to overcome the shortcomings of existing systems, the proposed exoskeleton glove was designed to satisfy two primary goals: (1) The weight and size of the total system should be small enough for it to be used in ADL's without fatigue and (2) The system should be capable of producing natural joint angles on the fingers and thumb during flexion and extension movements.

Figure 2 illustrates the major joints on a human hand. The fingers consist of three main joints, the metacarpophalangeal (MCP), proximal interphalangeal (PIP), and distal interphalangeal (DIP) joints, while the thumb contains the interphalangeal (IP) and MCP joints. In order to design an exoskeleton glove that satisfies the above mentioned goals, existing studies on human grasping motions, such as the common pinch, were reviewed [27–29]. In Ref. [30], experiments were performed to measure the joint angles for the index finger and thumb during a tip-pinch motion. The data showed that with a tip-pinch force of 100 g and a pulp distance of 1 cm, the index finger yielded joint angles of 49.1 deg (SD 9.5 deg), 41.0 deg (SD 10.7 deg), and 38.5 deg (SD 6.8 deg) for the MCP, PIP, and DIP joints, respectively, while the thumb yielded 12.8 deg (SD 9.4 deg), and 21.8 deg (SD 7.8 deg) for the MCP and IP joints. These data were used as a reference to design the exoskeleton glove.

A major conclusion drawn from these studies is the existence of inherent coupling of the human finger (MCP, PIP, and DIP joints) and thumb (IP and MCP joints). As a result of this coupling, the human fingers and thumbs essentially behave as single degree-of-freedom (DOF) systems while flexing and extending to perform common grasping motions. Making use of this factor in the design reduces the number of actuators needed, which in turn reduces the overall size and weight of the system.

The conceptual design for the proposed glove is inspired from the USC/Belgrade Robotic Hand [31]. The coupling mechanism used in this robotic hand was proven successful, so the approach was to adopt a similar coupling mechanism and modify it for suitable use in an exoskeleton glove. The proposed design for the glove mechanism consists of planar links that are connected by revolute joints, as detailed in Fig. 3.

The basic structure of the mechanism for the index finger is composed of links  $L_1$ ,  $L_2$ , and  $L_3$ , which correspond to the proximal, middle, and distal phalanges of the finger, respectively, as shown in Fig. 3. These three links are connected through three revolute joints,  $R_1$ ,  $R_2$ , and  $R_3$ . Specifically, links  $L_i$  and  $L_{i+1}$  are connected through revolute joint  $R_{i+1}$ . The constraint links  $C_1$  and  $C_2$  are used to produce the coupling relationship between the  $L_i$  links. Constraint link  $C_1$  connects link  $L_2$  to a fixed base frame (ground) by revolute joints  $Rc_1$  and  $Rc_2$ , while constraint link  $C_2$  connects links  $L_1$ – $L_3$  through joints  $Rc_3$  and  $Rc_4$ . The thumb mechanism is similar, containing only links  $L_1$  and  $L_2$ , which are connected by revolute joint  $R_2$ . The coupling action for the thumb mechanism is achieved by the constraint link  $C_1$ , which connects link  $L_2$  to the base frame through the revolute joints  $Rc_1$  and  $Rc_2$ .

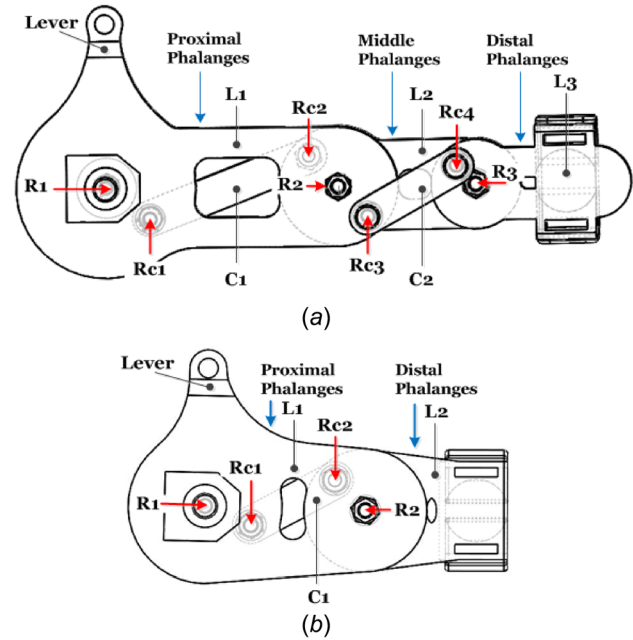


Fig. 3 Design of the mechanism (a) index finger and (b) thumb (both are shown for the left hand)

The assembly of the mechanisms shown in Fig. 3 can be summarized in the following steps:

- Link  $L_1$  is connected to the ground at joint  $R_1$ .
- Link  $L_1$  is connected to link  $L_2$  at joint  $R_2$ .
- Link  $L_2$  is connected to link  $L_3$  at joint  $R_3$  \*.
- Constraint link  $C_1$  connects to the ground at constraint joint  $Rc_1$  and to link  $L_2$  at constraint joint  $Rc_2$ .
- Constraint link  $C_2$  connects to link  $L_1$  at constraint joint  $Rc_3$  and to link  $L_3$  at constraint joint  $Rc_4$  \*.

Note: \* only applied for the finger mechanism and not for the thumb mechanism.

The flexion and extension motions are achieved when a rotary motion is applied at joint  $R_1$  by pushing and pulling on the lever of link  $L_1$ . This causes link  $L_1$  to bend and as it bends, the constraint links  $C_1$  and  $C_2$  translate the motion along to links  $L_2$  and  $L_3$ , as illustrated in Fig. 4. This collectively provides the coupling motion that reflects the natural flexion and extension of a human finger.

**2.1 Kinematic Modeling.** Before a detailed mechanical design of the exoskeleton glove could be created, the lengths of various links and positioning of revolute joints had to be determined based on the general dimensions of a human hand and the joint angles desired to be achieved in reference to Ref. [30]. To this extent, a kinematic modeling of the mechanism was performed. The modeling was done by taking into consideration the following design parameters (illustrated in Fig. 4):

- $l_i$ —length of link  $L_i$ , measured as the normal distance from  $R_i$  to  $R_{i+1}$ . For  $l_3$ , the distance is measured from  $R_3$  to the tip of the end effector/ $L_3$ .
- $c_i$ —length of constraint link  $C_i$ , measured as the normal distance from  $Rc_i$  to  $Rc_{i+1}$ .
- $\theta_i$ —joint angle of link  $L_i$ , defined as the angle measured from the  $x$ -axis of the base coordinate frame to the  $x$ -axis of the body coordinate frame.
- $d_i$ —the radial distance from constraint joint  $Rc_i$  to the origin of the corresponding link body coordinate frame.

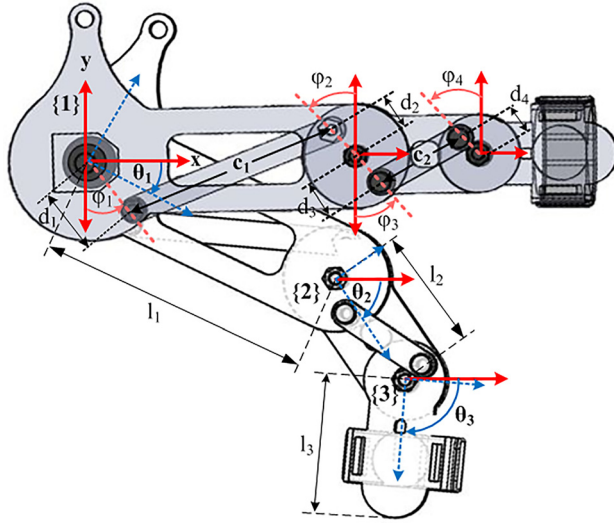


**Fig. 4** Index mechanism showing two configurations and the design parameters for kinematic modeling. The relaxed configuration is shown in gray, while the black and white schematic shows a flexion configuration.

- $\varphi_i$ —the angle made by constraint joint  $Rc_i$  with respect to the vertical  $y$ -axis of the body coordinate frame for link  $L_i$ , measured in the counterclockwise direction.

(Note:  $\varphi_2$  and  $\varphi_4$  are measured from the positive  $y$ -axis, while  $\varphi_1$  and  $\varphi_3$  are measured from the negative  $y$ -axis.)

The finger mechanism has three planar links with body coordinate frames attached to the joint, which are defined as  $[(x_1, y_1, \theta_1), (x_2, y_2, \theta_2), (x_3, y_3, \theta_3)]$ . The location of each link is represented by the  $x_i$  and  $y_i$  terms, while the  $\theta_i$  terms reflect the joint angles produced by the flexion/extension motions. These joint angles are measured from the  $x$ -axes of the original base coordinate frames of the links to the  $x$ -axes of the new body coordinate frames, which result from the mechanism being in motion. The base coordinate frame is illustrated in Fig. 4 by red coordinate lines ( $x, y$ ), while the body coordinate frames are shown by the blue dotted lines. All of the coordinate frames are right handed, with the  $z$ -axes pointing forward (out of the page).

The thumb mechanism on the other hand has two links, which are defined by the coordinates  $[(x_1, y_1, \theta_1), (x_2, y_2, \theta_2)]$ . For the single DOF mechanism for the index finger, establishing  $\theta_1$  as the input variable in the modeling yields the following eight constraint equations:

$$\begin{aligned}
 x_1 &= 0 \\
 y_1 &= 0 \\
 x_2 &= x_1 + l_1 \cos \theta_1 \\
 y_2 &= y_1 + l_1 \sin \theta_1 \\
 x_3 &= x_2 + l_2 \cos \theta_2 \\
 y_3 &= y_2 + l_2 \sin \theta_2 \\
 c_1^2 &= [x_2 - (d_2 \sin \varphi_2 \cos \theta_2 + d_2 \cos \varphi_2 \sin \theta_2) - d_1 \sin \varphi_1]^2 \\
 &\quad + [y_2 + (d_2 \cos \varphi_2 \cos \theta_2 - d_2 \sin \varphi_2 \sin \theta_2) + d_1 \cos \varphi_1]^2 \\
 c_2^2 &= [(x_3 - (d_4 \sin \varphi_4 \cos \theta_3 + d_4 \cos \varphi_4 \sin \theta_3)) \\
 &\quad - (x_1 + (l_1 + d_3 \sin \varphi_3) \cos \theta_1 + d_3 \cos \varphi_3 \sin \theta_1)]^2 \\
 &\quad + [(y_3 + (d_4 \cos \varphi_4 \cos \theta_3 - d_4 \sin \varphi_4 \sin \theta_3)) \\
 &\quad - (y_1 + (l_1 + d_3 \sin \varphi_3) \sin \theta_1 - d_3 \cos \varphi_3 \cos \theta_1)]^2
 \end{aligned} \tag{1}$$

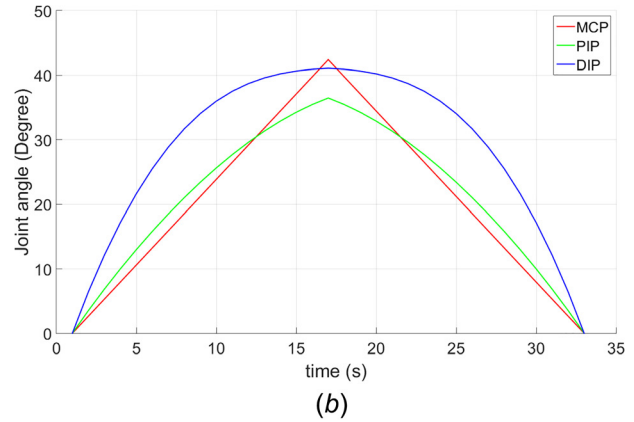
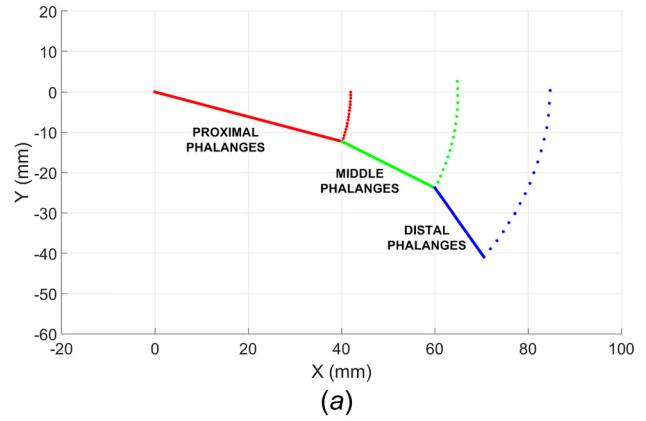


**Fig. 5** Simulation results (a) desired index finger trajectory starting at the origin of  $(0, 0)$  and (b) index finger joint angles

For the above equations, the constraint links  $C_i$  are considered to be absolute distance constraints. For the kinematic model, the link lengths  $L_i$  were set to general dimensions of a human hand. The other design parameters were estimated using a MATLAB simulation so that the joint angles achieved by the mechanism matched with the joint angles of a natural human finger. The design procedure for the thumb mechanism follows the same steps, but with only two main links  $L_i$  and one constraint link  $C_i$ . For the simulations, the joint angles were measured using the following relationships: (i) MCP joint =  $\theta_1$ , (ii) PIP joint (IP for thumb) =  $\theta_2 - \theta_1$ , and (iii) DIP joint =  $\theta_3 - \theta_2$ .

Figures 5 and 6 each present the kinematic simulation results using the estimated design parameters. For both simulations, the angles produced were negative, but for the sake of visualization, they are plotted as positive values. The index finger trajectory can provide maximum angles of 43 deg, 41 deg, and 37 deg for the MCP, PIP, and DIP joints, respectively, while the thumb trajectory offers MCP and IP angles of 19 deg and 17 deg, respectively. The simulated trajectories reflect the natural joint relationship of the index finger and thumb during the 100 g tip-pitch motion, shown in Figs. 5(a) and 6(a), respectively. These modeling results confirm that the each mechanism is capable of enforcing joint angles resembling that of a natural human hand.

### 3 Electro-Mechanical Design

**3.1 Actuation.** To achieve flexion and extension motions with adequate speed and force, Bimba double acting pneumatic actuators were used for the index finger and thumb mechanisms of the exoskeleton glove. With these actuators, the glove can complete flexion and extension motions within 1 s with a force of 10 N. The complete pneumatic system consists of an air

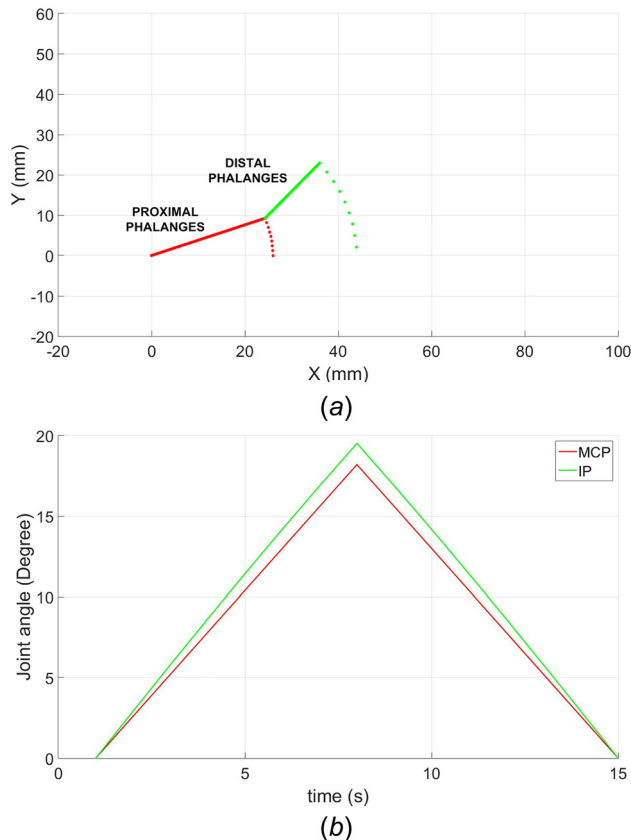


**Fig. 6 Simulation results (a) desired thumb trajectory starting at the origin of (0, 0) and (b) thumb joint angles**

compressor (150 PSI), a 0.5 gallon air reservoir, a pressure regulator, air tubing, and solenoid valves by SMC Corporation, which control the air flow into the pneumatic actuators.

**3.2 Sensors.** For absolute position sensing, Bourns rotary encoders were placed on each of the finger and thumb mechanisms at the  $R_1$  joints, which correspond to the MCP joints on the human hand. The readings from the electrical encoders correspond to the angular position of the  $L_1$  links of the finger and thumb mechanisms. A digital protractor was used to manually calibrate the encoder values into angle measurements. The remaining joint angles of the PIP and DIP joints of the index finger and the IP joint of the thumb are calculated using the kinematic model of the mechanism. Using the kinematic model, the position of the final link that corresponding to the distal phalanges of the finger and thumb can also be calculated.

Force sensitive resistors (FSR) by Interlink Electronics were used to measure the amount of force being applied on the index finger and thumb by the exoskeleton frames during grasping. These FSR sensors have a continuous analog resolution and a force sensitivity range of 0.2 N–20 N. Two force sensors are placed on each of the finger/thumb tip pieces, as shown in Fig. 7. The force sensors were calibrated using known weights.

In addition to the sensors, vibration motors were added to the design in order to provide feedback to the user. This feedback can be used in several applications such as providing haptic feedback for virtual reality applications, acting as a stimulus to prompt the user to perform certain tasks for rehabilitation, or as feedback for tele-navigation [3]. The motors used were Adafruit mini vibration motors, which are rated for 5V max with a current draw of 100 mA. The motors have a weight of 0.9 g and can provide a vibration sensation that resembles that of a standard mobile phone vibrating unit.

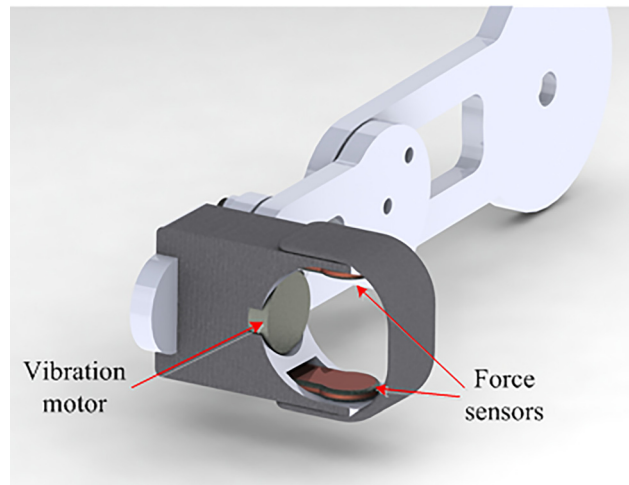


**Fig. 7 Design of the tip holder shown on finger mechanism (same for thumb mechanism)**

## 4 Prototype Integration

The basic mechanisms shown in Fig. 3 were further developed into a detailed design for the two-digit prototype. The detailed design of the system is shown in Fig. 1. The mechanisms for the index finger and the thumb were three-dimensional (3D) printed separately using acrylonitrile butadiene styrene plastic and then connected together using a base plate. The base plate, which supports the weight of the two mechanisms and the actuators, was strapped onto the back of the hand using elastic Velcro straps. This allows for the adjustment of the exoskeleton glove to suit different hand sizes. The prototype weighs 24 g, making it lightweight as compared to the two finger exoskeleton of Ref. [32], which weighs 180 g. To complete the prototype implementation, a circuit board and software interface were developed to control the glove and all integrated sensors. The circuit board and pneumatic system were kept separate so that they could be either incorporated into a backpack or kept on a table while the exoskeleton glove was being used.

**4.1 Electrical Circuit.** A custom printed circuit board (PCB) was developed to connect the sensors and actuators with the microcontroller unit and other electrical components. The force sensors and encoders were connected to the microcontroller unit as inputs while the pneumatic actuators and vibration motors were the output connections. The pneumatic actuators were controlled using the solenoid valves to produce a linear actuation. The microcontroller itself powers these solenoid valves on/off via N-MOSFET switches. The vibration motors are directly connected to a motor driver since the current ratings of these motors exceed the tolerance of the microcontroller input/output (I/O) pins. The microcontroller connects to the motor driver with two enable pins for each vibration motors, one for the index finger and another for the thumb.

A Teensy 3.1 board serves as the microcontroller unit for the system. It is rated at a clock frequency of 72 MHz, which provides sufficient speed for acquiring sensor data from the encoders and force sensors while performing commands to control the vibration motors and the actuation for flexion or extension of the index and thumb.

In addition to the sensors and motors, the PCB contains three tactile pushbuttons. One pushbutton serves as the main power switch while the other two are used for actuation controls. One of these two is used to depressurize the pneumatic actuators to allow free movements among the finger and thumb. The last button is used to trigger an automatic flexion and extension motion on both

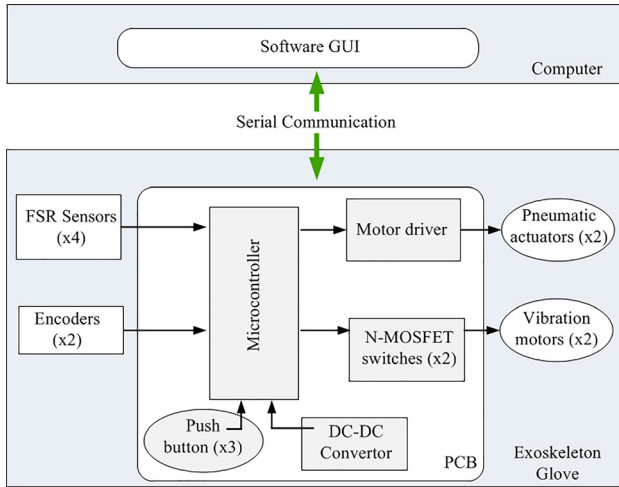


Fig. 8 System architecture of exoskeleton glove

the finger and thumb to perform a grasp. This feature allows the exoskeleton device to serve as a standalone device for different applications such as rehabilitation. For full feature controls, the PCB can be interfaced with the graphical user interface (GUI) for the exoskeleton glove system that provides additional commands and functionalities. The overall architecture of the exoskeleton glove system is demonstrated in Fig. 8.

**4.2 Software GUI.** The exoskeleton GUI is an executable application developed in MATLAB. This software provides additional commands to control the glove and functionalities for data analysis. To control the glove actuation, the commands are divided into the following groups: index finger controls, thumb controls, and both the index finger and thumb together. Each of these control groups consists of the following commands to control only the specified finger/thumb: trigger motion, release, and vibrate pulse. The index and thumb combined control group contains these same commands as well as additional commands such as the auto trigger and release pinch command, which actuates the index finger and thumb to perform a pincer grasp and then releases the pinch after a time delay of 1.50 s. For all three control groups, the vibrate pulse commands were programmed to turn on the corresponding vibrate motors for 0.5 s. The GUI commands for actuating the pinching motions for each digit are accomplished by signaling the microcontroller to power the solenoid valves on and off accordingly, as mentioned in Sec. 4.1.

While reading in the sensor data, the GUI displays the FSR sensor data in terms of Newtons (N) and the encoder data in degrees for both the index and thumb. For analysis purposes, the GUI has a record feature that will capture sensor data at a rate of 20 Hz and store the data into a microsoft excel file. An additional feature of the GUI includes an imported SOLIDWORKS CAD model of a human hand. The CAD model was incorporated to serve as a real-time animation showing the movements of the user's hand while using the glove.

## 5 Experimental Validation

An experiment was conducted to verify whether the joint angles enforced on the index finger and thumb by the glove during flexions and extensions reflect the desired trajectories for obtaining natural joint coupling. The experiment involved mounting the exoskeleton glove on a wooden mannequin hand and tracking the motions of index finger and thumb, which were produced by the glove, as shown in Fig. 9. The tracking was achieved using a GoPro HERO5 Session 10MP camera with 4K video resolution. To capture the finger and thumb at various stages during motions, the

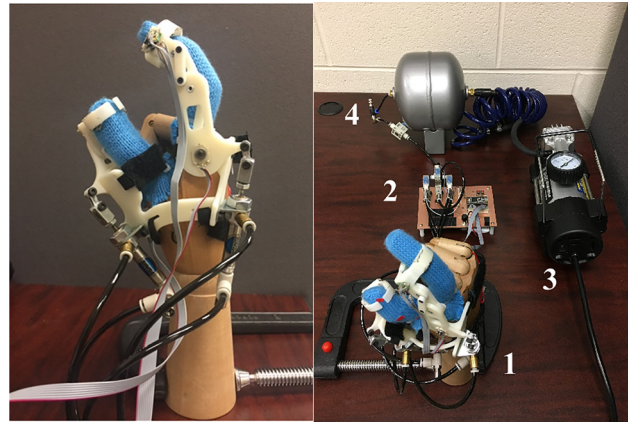


Fig. 9 Experimental setup for the prototype: 1—exoskeleton glove on mannequin, 2—embedded controller, 3—compressor, 4—air tank

camera was set up to record videos at 30 frames per seconds. A MATLAB script was programmed to utilize basic computer vision techniques to analyze the captured images. The code first identifies red markers placed on the MCP, PIP, and DIP joints and MCP and IP joints of the inserted index finger and thumb, respectively. Once these red markers were identified, the centroids of the markers were computed to determine the centers of the joints. Line segments were drawn between the joint centers such that the corresponding joint angles could be calculated (illustrated in Fig. 10). Thus, from identifying the red markers from image to image, the overall joint angles were calculated and used to analyze the joint coupling relationships enforced by the exoskeleton glove.

Although the GoPro camera is equipped with an ultrawide angle lens that has reduced distortion, it was still necessary to apply a distortion correction filter to each of the video image frames prior to the joint tracking procedure. In order to accomplish this, a camera calibration was performed using the traditional method of capturing several pictures of a standard checkerboard pattern using the subject camera [33]. The distorted images of the checkerboard were then analyzed using the MATLAB camera calibration toolbox to compute the camera intrinsic, extrinsic, and lens-distortion parameters. These parameters were used for the undistortion filtering.

To overcome the lack of inherent coupling between the respective thumb and index finger joints of the mannequin hand, the



Fig. 10 Experimental analysis at various stages of the bending motion: (a) index finger and (b) thumb

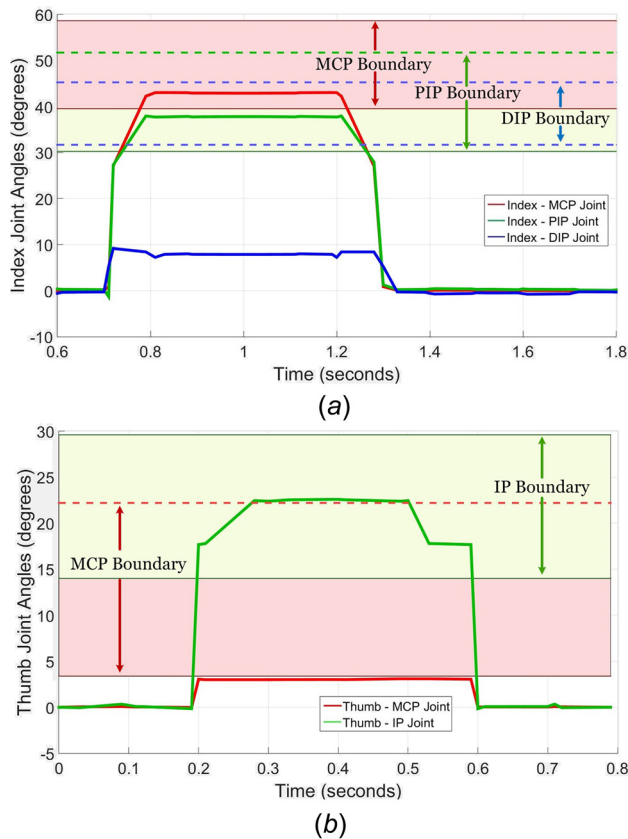


**Fig. 11** Experimental results for (a) index finger joints and (b) thumb joints

index finger and thumb were inserted into a cloth glove as shown in Fig. 10. This allows for the joints to bend in correlation, when the mechanisms for index finger and thumb apply force at the distal phalange of the corresponding finger/thumb.

The experiment for each digit was performed independently of one another. The results from these experiments are plotted in Fig. 11, which displays the calculated joint angles for both digits with respect to time. The MCP, PIP, and DIP joints of the index finger bend at average angle of 42.9 deg, 37.8 deg, and 8.01 deg, respectively, while the MCP and IP joints of the thumb bend 3.01 deg and 22.5 deg, respectively. To verify the coupling relationships of the joints, the results were compared to the targeted natural angles from Ref. [30], which were previously mentioned in Sec. 2. Figure 11 displays the comparisons by plotting the resulting joint angles against the acceptable ranges of the natural joint angular displacements. More specifically, the experimentally derived upper and lower bounds for the natural joint angles for a tip-pinch force of 100 g (1 cm pulp distance) were computed by adding and subtracting the standard deviation with the joint angle averages [30]. These upper and lower boundaries serve as the range of acceptable variations for each of joint angle maximums.

As seen from Fig. 11, the angular displacements for the MCP and PIP joints of the index finger were well within their acceptable range for natural angular displacements at the end of the pinch. However, the final angular displacement for the DIP joint of the index finger fell short from reaching within its perspective boundary by 23.7 deg. The MCP angular joint displacement for the thumb fell within its range while the IP joint was on the boundary of the acceptable range, falling short by 0.4 deg.

The shortcoming of the index finger DIP joint angle was due to the misalignment of the Velcro fingertip holder. Instead of being positioned at the distal phalange region of the mannequin hand,

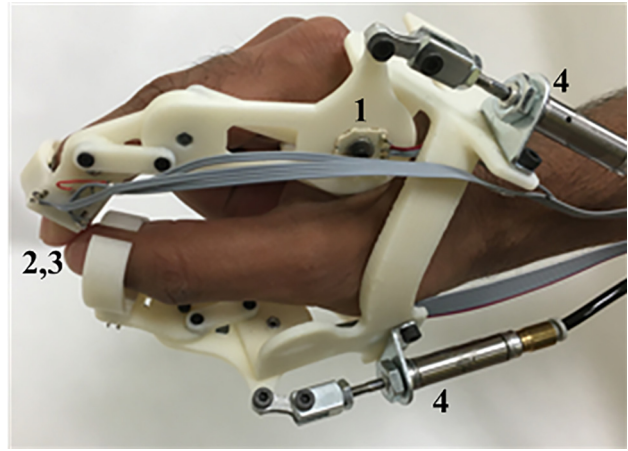


**Fig. 12** Prototype on a human hand: 1—absolute position sensor, 2—FSR sensor, 3—vibration motor, and 4—pneumatic actuator

the holder was located near the DIP joint. This misalignment was due to the size difference between the mannequin hand and the human hand, for which the holder piece was originally designed to accommodate. The mannequin fingers were longer (index finger by 3 cm and thumb by 1 cm) than that of an average human hand and as a result, the mechanism was able to slide down the mannequin finger during the bending movements of the experiment. The same reason applies to the IP joint angles of the thumb coming short of the acceptable range. The glove can be seen properly worn on a human hand in Fig. 12.

Overall, the pincer grasp was achieved in 0.63 s, with 0.1 s for the pinch, 0.41 s to hold the pinch, and another 0.12 s for releasing. Despite the experimental shortcoming of the DIP joint of the index finger, the results demonstrated that the joint angles produced by the exoskeleton resemble natural bending trajectories of the human hand during grasping motions, such as the pincer grasp.

## 6 Design Improvements and Future Work

**6.1 Motivation.** Although the proposed design produced promising results in being a lightweight hand exoskeleton that can emulate natural joint angles, improvements will be needed to expand this proof of concept into a fully functional assistive device that would be sufficient for ADLs. Some of these shortcomings are listed below:

- *Actuation:* Even though the pneumatic actuation method offers speed and power, it lacks the ease of controllability. Specifically, pneumatic actuators naturally allow for two basic configurations: full flexion and full extension of the hand exoskeleton digits (fully open glove and fully closed). To allow for efficient grasping of the various objects that humans interact with daily, the hand exoskeleton must have the ability to conform to the shape of the object being grasped. This therefore requires the actuation system to be able to achieve any of the infinite configurations between the range of maximum flexion and maximum extension.
- *Force feedback.* With the human hand being a complex structure with many capabilities, it can offer a variety of grasps and pinches. These grasps differ according to the joint angles, trajectories, and orientations of the fingers and thumb and the overall output grip force. To control various grasps at high precision when interacting with objects or completing tasks, the human hand incorporates sensory processing with its motor skills. This allows the human hand to receive force feedback across many nerves within

the hand at high level of sensitivity and react accordingly. Although the proposed design contains force sensors that can measure interactive forces, it lacks the ability to use this force information as feedback input for controlling the force, speed, and ending trajectories of each finger and thumb of the hand exoskeleton. Without the hand exoskeleton having this type of compliance functionality, it will not be able to adjust the strength of its grasp and finger trajectories.

- **Portability.** When designing a hand exoskeleton that can primarily serve as an assistive glove or as a haptic device, portability becomes a major design parameter. The use of a pneumatic actuation system does not achieve this design goal however. As shown in Fig. 9, pneumatic actuators require items such as an air tank and compressor to create a fully functional system, which are not ideal to carry around for an extended period of time. Another solution may be to have a smaller air tank and compact compressor that could fit inside a backpack for the user to wear, thus making the pneumatic system portable. Despite this being a plausible approach, it creates the concerns of having less available air for the pneumatic actuators to use between refills and adds more weight for the user to carry, thereby introducing serious issues for the elderly and disabled. As a proof of concept for the proposed design, the pneumatic actuation was sufficient for experimental validation. But for a portable system, the actuation system has to be redesigned possibly with miniature light weight DC motors powered by LiPo batteries.

In order to address the shortcomings of the proposed design, future versions of the prototype will replace the pneumatic actuation system with electrical actuators using a series elastic actuator (SEA) design. SEAs are commonly used to achieve force control in robotic systems that interact with the environment. SEAs can be implemented by placing an elastic element, such as a torsional or compression spring in series between the drive train of an actuator and its payload, thereby creating a compliant actuation unit. In addition to being essential for the SEA design, the use of electrical actuators in place of the pneumatic system makes the system more portable. By shifting toward an electrical actuation system, the hand exoskeleton will be able to achieve desired forces and speeds while being powered by lightweight and high energy density LiPo batteries. In the section below, the motivation for SEAs is explained and the proposed design is presented in detailed.

**6.2 SEA Design.** An ideal actuation unit for a force controllable robotic system is one that can perfectly output the desired force, regardless of any inertia produced from the movement of the payload. Despite the advancement in technology, modern actuators possess several limitations that hinder them from being perfect candidates for force control. Some of these limitations include: mechanical impedance, stiction friction, and low actuator mechanical bandwidth [34]. Impedance in the actuator is due to the inertia or additional forces that are created by the load motion. This force is reflected onto the overall output force from the actuator, which can introduce errors in efficiently achieving the desired force. Like many other robotic systems, the proposed design contains several mechanical components that slide against each other. This sliding behavior results in stiction friction. In order to overcome the resistance due to stiction friction, the actuator has to exert a higher breakaway force, which in return limits the minimum force the actuator can output. This in turn leads to the issue of low bandwidth due to the mechanical stiffness and power saturation of the actuation module.

Series elastic actuators serve to overcome these issues due to the elasticity factor which allows for storing energy while also introducing shock tolerance within the system. Not only does it help with making the system more compliant with the

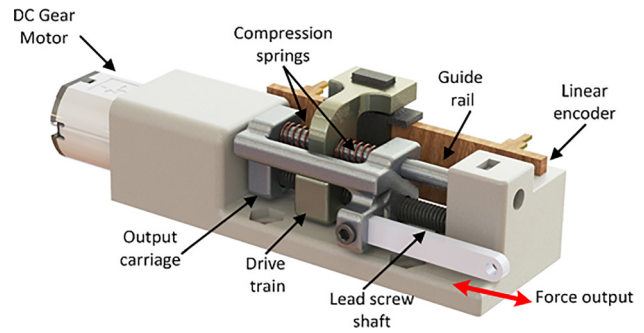


Fig. 13 Proposed SEA design

environment, but the tolerance also allows for the actuation unit to be more back drivable. As a result, this lowers the amount of impedance in the system and the mechanical stiffness that negatively impacts the force bandwidth. Most importantly, SEA offers a way to achieve force control by means of primarily controlling position using Hooke's law [34,35]. In most cases, position is easier to control accurately in motors that use gear trains or have feedback encoders attached. Overall, SEAs utilize active sensing and closed-loop controls to reduce the disturbances from friction and inertia to ultimately achieve the desired force output.

The design of the proposed SEA is detailed in Fig. 13. The design uses a geared DC motor with a leadscrew acting as the shaft. The geared DC motor offers a high torque, at sufficiently low speed. The leadscrew shaft allows for the translation of rotary motion into linear motion, reflecting the original linear drive of the pneumatic actuators. The design was adapted from the traditional SEA design done by Pratt et al. [34]. The overall actuation unit consists of three major components: a drive train, output carriage, and compression springs. The drive-train component houses a ball nut that attaches to the leadscrew shaft, allowing the entire drive-train unit to move forward and backward along the shaft as the motor rotates clockwise and counterclockwise, respectively. The drive-train component is coupled with the output carriage unit by the placement of compression springs between both components. Specifically, the drive-train component is placed between both ends of the output carriage unit. A compression spring is placed on each side of the drive train, establishing springs between the drive train and output carriage on both sides. Therefore, as the drive-train component moves forward and backward along the leadscrew, the compression springs push and pull against the output carriage component, causing it to move in synchronization with the drive-train component. The overall output force from the leadscrew motor and compression springs is reflected onto the output carriage unit. This force on the output carriage is used to push the lever of the finger/thumb mechanism. To align all of the components together during motion, a guide rail is installed above the leadscrew shaft.

During operation, the output forces can be measured through the deflection of the compression springs. To measure the spring deflection, a linear encoder is incorporated into the SEA design by

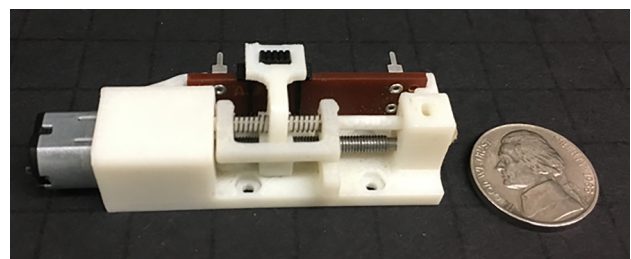
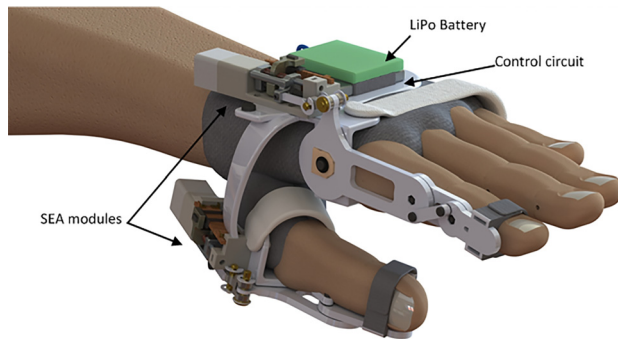


Fig. 14 3D printed prototype of SEA module



**Fig. 15 Proposed exo-glove design with electric actuation and SEA**

attaching the scale of the encoder onto the drive-train component, as shown in Fig. 13. This attachment allows the scale of the encoder to move in accordance with the drive train for tracking its position. Using the absolute rotary encoders that are placed onto the glove mechanisms at the MCP joint of the fingers and thumb, the position for the output carriage piece can also be tracked. As a result, the deflection of the springs can be calculated using the positioning information for both the drive train and the output carriage components. By optimizing the stiffness of the springs, the desired force bandwidth and sensitivity can be attained from the SEA unit [34]. A prototype of the proposed SEA design was 3D printed and is shown in Fig. 14. By equipping both the index finger and thumb mechanism of the proposed hand exoskeleton with the SEA actuation unit as shown in Fig. 15, the exoskeleton glove will be able to grasp objects of various shapes and strengths while maintaining a stable grip through force control.

## 7 Conclusion

The paper presented the design and integration of a two-digit prototype of an exoskeleton glove that was proposed to address the commonly encountered large size, heavy weight, and unnatural coupling issues of traditional hard and soft exoskeleton gloves. The design of the exoskeleton glove allows for the finger and thumb mechanisms to be attached alongside the respective finger/thumb, decreasing the size of the exoskeleton glove as well as reducing the discomfort caused from using larger and heavier traditional gloves. Mathematical modeling of the design was presented and the proposed concept was validated through experiments. Results showed the potential of the exoskeleton glove to achieve natural coupling among the joints to resemble that of a human hand. Although the initial features of the prototype to record finger and thumb movements, measure exerted forces on the glove, and provide vibrational feedback, make it suitable for multiple applications, the pneumatic actuators present several shortcomings that affect performance. These shortcomings were analyzed and a feasible solution was presented, which proposed using SEAs as alternative actuation methods. The proposed SEA design was further developed into a proof-of-concept prototype.

Future work will involve implementing force feedback and control with the proposed SEA prototype. In addition, the two-digit design will be extended into a full hand exoskeleton glove by modifying the index finger mechanism to accommodate for the additional fingers. The overall grasping performance with force control will be investigated using the full hand exoskeleton glove.

## References

[1] MANUS VR, 2014, "The Pinnacle of VR Controllers," MANUS VR, Eindhoven, The Netherlands, accessed Dec. 26, 2017, [www.manus-vr.com](http://www.manus-vr.com)

[2] CyberGlove Systems, 2009, "CyberGrasp," CyberGlove Systems Inc., San Jose, CA, accessed Sept. 14, 2017, <http://www.cyberglovesystems.com/cybergrip/>

[3] Tatsumi, H., Murai, Y., Sekita, I., Tokumasu, S., and Miyakawa, M., 2016, "Cane Walk in the Virtual Reality Space Using Virtual Haptic Sensing: Toward

Developing Haptic VR Technologies for the Visually Impaired," IEEE International Conference on Systems, Man, and Cybernetics (SMC), Kowloon, China, Oct. 9–12, pp. 2360–2365.

[4] Ito, S., Kawasaki, H., Ishigure, Y., Natsume, M., Mouri, T., and Nishimoto, Y., 2011, "A Design of Fine Motion Assist Equipment for Disabled Hand in Robotic Rehabilitation System," *J. Franklin Inst.*, **348**(1), pp. 79–89.

[5] Teixeira, C. D. C., Marx, F. C., and De Oliveira, J. C., 2016, "A Haptic Rehabilitation System," 18th Symposium on Virtual and Augmented Reality (SVR), Gramado, Brazil, June 21–24, pp. 188–192.

[6] Heo, P., Gu, G. M., Jin Lee, S., Rhee, K., and Kim, J., 2012, "Current Hand Exoskeleton Technologies for Rehabilitation and Assistive Engineering," *Int. J. Precis. Eng. Manuf.*, **13**(5), pp. 807–824.

[7] Ma, Z., and Ben-Tzvi, P., 2013, "Tendon Transmission Efficiency of a Two-Finger Haptic Glove," IEEE International Symposium on Robotic and Sensors Environments (ROSE), Washington, DC, Oct. 21–23, pp. 13–18.

[8] Ho, N. S. K., Tong, K. Y., Hu, X. L., Fung, K. L., Wei, X. J., Rong, W., and Susanto, E. A., 2011, "An EMG-Driven Exoskeleton Hand Robotic Training Device on Chronic Stroke Subjects: Task Training System for Stroke Rehabilitation," IEEE International Conference on Rehabilitation Robotics (ICORR), Zurich, Switzerland, June 29–July 1, pp. 1–5.

[9] Iqbal, J., Khan, H., Tsagarakis, N. G., and Caldwell, D. G., 2014, "A Novel Exoskeleton Robotic System for Hand Rehabilitation—Conceptualization to Prototyping," *Biocybern. Biomed. Eng.*, **34**(2), pp. 79–89.

[10] Arata, J., Ohmoto, K., Gassert, R., Lamberg, O., Fujimoto, H., and Wada, I., 2013, "A New Hand Exoskeleton Device for Rehabilitation Using a Three-Layered Sliding Spring Mechanism," IEEE International Conference on Robotics and Automation (ICRA), Karlsruhe, Germany, May 6–10, pp. 3902–3907.

[11] Worsnopp, T. T., Peshkin, M. A., Colgate, J. E., and Kamper, D. G., 2007, "An Actuated Finger Exoskeleton for Hand Rehabilitation Following Stroke," IEEE Tenth International Conference on Rehabilitation Robotics (ICORR), Noordwijk, The Netherlands, June 13–15, pp. 896–901.

[12] Takagi, M., Iwata, K., Takahashi, Y., Yamamoto, S. I., Koyama, H., and Komeda, T., 2009, "Development of a Grip Aid System Using Air Cylinders," IEEE International Conference on Robotics and Automation (ICRA), Kobe, Japan, May 12–17, pp. 2312–2317.

[13] Ertas, I. H., Hocaoglu, E., Barkana, D. E., and Patoglu, V., 2009, "Finger Exoskeleton for Treatment of Tendon Injuries," 11th IEEE International Conference on Rehabilitation Robotics (ICORR), Kyoto, Japan, June 23–26, pp. 194–201.

[14] Hasegawa, Y., Mikami, Y., Watanabe, K., and Sankai, Y., 2008, "Five-Fingered Assistive Hand With Mechanical Compliance of Human Finger," IEEE International Conference on Robotics and Automation (ICRA), Pasadena, CA, May 19–23, pp. 718–724.

[15] Zhou, M. A., Ben-Tzvi, P., and Danoff, J., 2015, "Hand Rehabilitation Learning System With an Exoskeleton Robotic Glove," *IEEE Trans. Neural Syst. Rehabil. Eng.*, **24**(12), pp. 1323–1332.

[16] Ben-Tzvi, P., Danoff, J., and Ma, Z., 2016, "The Design Evolution of a Sensing and Force-Feedback Exoskeleton Robotic Glove for Hand Rehabilitation Application," *ASME J. Mech. Rob.*, **8**(5), p. 051019.

[17] Ben-Tzvi, P., and Ma, Z., 2015, "Sensing and Force-Feedback Exoskeleton (SAFE) Robotic Glove," *IEEE Trans. Neural Syst. Rehabil. Eng.*, **23**(6), pp. 992–1002.

[18] Ma, Z., and Ben-Tzvi, P., 2011, "An Admittance-Type Haptic Device—RML Glove," *ASME Paper No. IMECE2011-64108*.

[19] Ma, Z., and Ben-Tzvi, P., 2015, "Design and Optimization of a Five-Finger Haptic Glove Mechanism," *ASME J. Mech. Rob.*, **7**(4), p. 041008.

[20] In, H., and Cho, K., 2015, "Exo-Glove: Soft Wearable Robot for the Hand Using Soft Tendon Routing System," *IEEE Rob. Autom.*, **22**(1), pp. 97–105.

[21] Lee, S. W., Landers, K. A., and Park, H. S., 2014, "Development of a Biomimetic Hand Exotendon Device (BiomHED) for Restoration of Functional Hand Movement Post-Stroke," *IEEE Trans. Neural Syst. Rehabil. Eng.*, **22**(4), pp. 886–898.

[22] Nycz, C. J., Delph, M. A., and Fischer, G. S., 2015, "Modeling and Design of a Tendon Actuated Soft Robotic Exoskeleton for Hemiparetic Upper Limb Rehabilitation," Annual International Conference of the IEEE Engineering in Medicine and Biology Society (EMBC), Milan, Italy, Aug. 25–29, pp. 3889–3892.

[23] Hasegawa, Y., Tokita, J., Kamibayashi, K., and Sankai, Y., 2011, "Evaluation of Fingertip Force Accuracy in Different Support Conditions of Exoskeleton," IEEE International Conference on Robotics and Automation (ICRA), Shanghai, China, May 9–13, pp. 680–685.

[24] Koo, I., Byunghyun Kang, B., and Cho, K.-J., 2013, "Development of Hand Exoskeleton Using Pneumatic Artificial Muscle Combined With Linkage," *J. Korean Soc. Precis. Eng.*, **11**(11), pp. 1217–1224.

[25] Polygerinos, P., Wang, Z., Galloway, K. C., Wood, R. J., and Walsh, C. J., 2015, "Soft Robotic Glove for Combined Assistance and At-Home Rehabilitation," *Rob. Auton. Syst.*, **73**, pp. 135–143.

[26] Tadano, K., Akai, M., Kadota, K., and Kawashima, K., 2010, "Development of Grip Amplified Glove Using Bi-Articular Mechanism With Pneumatic Artificial Rubber Muscle," IEEE International Conference on Robotics and Automation (ICRA), Anchorage, AK, May 3–7, pp. 2363–2368.

[27] Liu, M., and Xiong, C., 2014, "Synergistic Characteristic of Human Hand During Grasping Tasks in Daily Life," International Conference on Intelligent Robotics and Applications (ICIRA), Guangzhou, China, Dec. 17–20, pp. 67–76.

[28] Hook, W. E., and Stanley, J. K., 1986, "Assessment of Thumb to Index Pulp to Pulp Pinch Grip Strengths," *J. Hand Surg. Am.*, **11**(1), pp. 91–92.

- [29] Hemmi, K., and Inoue, K., 2000, "A Proposal of Three Dimensional Movement Model for Index Finger and Thumb," Fourth Asia-Pacific Conference on Control and Measurement, Guilin, China, July 9–12, pp. 241–246.
- [30] Hara, A., Yamauchi, Y., and Kusunose, K., 1994, "Analysis of Thumb and Index Finger Joints During Pinching Motion and Writing a Cross, as Measured by Electrogoniometers," *Clinical Biomechanics and Related Research*, Y. Hirasawa, C. B. Sledge, and S. L.-Y. Woo, eds., Springer, Tokyo, Japan, pp. 282–293.
- [31] Bekey, G. A., Tomovic, R., and Zeljkovic, I., 1990, "Control Architecture for the Belgrade/USC Hand," *Dexterous Robot Hands*, S. T. Venkataraman and T. Iberall, eds., Springer, New York, pp. 136–149.
- [32] Ma, Z., and Ben-Tzvi, P., 2015, "RML Glove-an Exoskeleton Glove Mechanism With Haptics Feedback," *IEEE/ASME Trans. Mechatronics*, **20**(2), pp. 641–652.
- [33] Yu, C., and Peng, Q., 2006, "Robust Recognition of Checkerboard Pattern for Camera Calibration," *Opt. Eng.*, **45**(9), p. 93201.
- [34] Pratt, J., Krupp, B., Morse, C., Pratt, J., and Krupp, B., 2002, "Feature Series Elastic Actuators for High Fidelity Force Control," *Ind. Rob: Int. J.*, **29**(3), pp. 234–241.
- [35] Pratt, G. A., and Williamson, M. M., 1995, "Series Elastic Actuators," *IEEE/RSJ International Conference on Intelligent Robots and Systems*, Pittsburgh, PA, Aug. 5–9, pp. 399–406.